

Colossal dielectric permittivity in (Al + Nb) co-doped rutile SnO₂ ceramics with low loss at room temperature

Yongli Song, Xianjie Wang^{*}, Xingquan Zhang, Xudong Qi, Zhiguo Liu, Lingli Zhang, Yu Zhang, Yang Wang, Yu Sui^{*}, and Bo Song^{*}

Citation: *Appl. Phys. Lett.* **109**, 142903 (2016); doi: 10.1063/1.4964121

View online: <http://dx.doi.org/10.1063/1.4964121>

View Table of Contents: <http://aip.scitation.org/toc/apl/109/14>

Published by the [American Institute of Physics](#)

Articles you may be interested in

[Direct view at colossal permittivity in donor-acceptor \(Nb, In\) co-doped rutile TiO₂](#)

Appl. Phys. Lett. **109**, 092906092906 (2016); 10.1063/1.4962219

[Simultaneous observation of up/down conversion photoluminescence and colossal permittivity properties in \(Er +Nb\) co-doped TiO₂ materials](#)

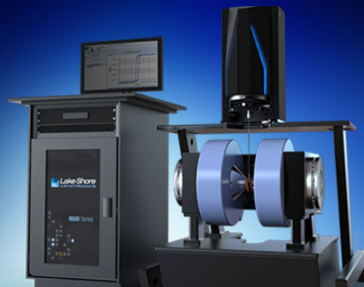
Appl. Phys. Lett. **109**, 042903042903 (2016); 10.1063/1.4959829

[Microstructure and dielectric properties of \(Nb + In\) co-doped rutile TiO₂ ceramics](#)

Appl. Phys. Lett. **116**, 074105074105 (2014); 10.1063/1.4893316




Lake Shore
CRYOTRONICS



NEW 8600 Series VSM

For fast, highly sensitive
measurement performance

LEARN MORE 

Colossal dielectric permittivity in (Al + Nb) co-doped rutile SnO₂ ceramics with low loss at room temperature

Yongli Song,¹ Xianjie Wang,^{1,a)} Xingquan Zhang,² Xudong Qi,¹ Zhiguo Liu,¹ Lingli Zhang,¹ Yu Zhang,¹ Yang Wang,^{1,3} Yu Sui,^{1,a)} and Bo Song^{1,3,a)}

¹Department of Physics, Harbin Institute of Technology, Harbin 150001, China

²Analytical and Testing Center, Southwest University of Science and Technology, Mianyang 621010, China

³Academy of Fundamental and Interdisciplinary Sciences, Harbin Institute of Technology, Harbin 150001, China

(Received 31 July 2016; accepted 20 September 2016; published online 4 October 2016)

The exploration of colossal dielectric permittivity (CP) materials with low dielectric loss in a wide range of frequencies/temperatures continues to attract considerable interest. In this paper, we report CP in (Al + Nb) co-doped rutile SnO₂ ceramics with a low dielectric loss at room temperature. Al_{0.02}Nb_{0.05}Sn_{0.93}O₂ and Al_{0.03}Nb_{0.05}Sn_{0.92}O₂ ceramics exhibit high relative dielectric permittivities (above 10³) and low dielectric losses (0.015 < tan δ < 0.1) in a wide range of frequencies and at temperatures from 140 to 400 K. Al doping can effectively modulate the dielectric behavior by increasing the grain and grain boundary resistances. The large differences in the resistance and conductive activation energy of the grains and grain boundaries suggest that the CP in co-doped SnO₂ ceramics can be attributed to the internal barrier layer capacitor effect. *Published by AIP Publishing.*
<http://dx.doi.org/10.1063/1.4964121>

The compounds with a colossal dielectric permittivity (CP > 10³) have attracted a lot of attention because of their applications in high-energy density storage and microelectronics as a result of the continually increasing demands of microelectronics applications.^{1–4} Ferroelectric CP materials, such as BaTiO₃,^{5,6} Bi_{0.5}Na_{0.5}TiO₃,⁷ (K,Na)NbO₃,⁸ and (1-x)[Pb(Mg_{1/3}Nb_{2/3})O_{3-x}[PbTiO₃]] (PMN-PT),^{9,10} have been widely studied; however, the CP can only be achieved in a small temperature range around the Curie temperature, which limits their application. CP has been reported across a wide range of temperatures in the traditional non-ferroelectric materials, such as CaCu₃Ti₄O₁₂ (CCTO),^{2,11} doped NiO,¹² La_{2-x}Sr_xNiO₄,^{13,14} and ZnO,^{15,16} however, the dielectric loss in these materials is too high (>0.1) to be applied. Although doped CCTO¹⁷ and doped Y_{2/3}Cu₃Ti₄O₁₂ (Ref. 18) show CP with low dielectric loss, the low dielectric loss can only be achieved in a narrow frequency range. Recently, Hu *et al.* found that In + Nb co-doped rutile TiO₂ ceramics exhibit CP with low dielectric loss (~0.05) over a very broad range of temperatures/frequencies,¹⁹ but the low dielectric loss strongly depends on the synthesis conditions.^{20–23} Therefore, new CP materials with low dielectric loss over a wide range of temperatures and frequencies are still being investigated.

Doped SnO₂ was investigated as a kind of varistor with insulating grain boundaries and semi-conducting grains, similar to CCTO and doped TiO₂ ceramics in which CP was discovered.^{24–27} CP was also observed in doped SnO₂ ceramics; however, CP can only be observed at low frequencies in Zn+Co co-doped SnO₂ ceramics.²⁸ Nb doping can generate n-type carriers that can result in CP and high dielectric loss in tetravalent oxides. Trivalent cation doping can be

considered acceptor doping and can capture the electrons introduced by Nb doping in tetravalent oxides. As a result, the concentration of carriers can be acutely tuned by adjusting the ratio between Nb and trivalent cations, which will result in different grain and grain boundary resistances for co-doped tetravalent oxides.^{29,30} Therefore co-doped SnO₂ may be a type of CP material with low dielectric loss.

In this paper, we investigated the dielectric properties of Al + Nb co-doped rutile SnO₂ ceramics. CP (~10³) with a low dielectric loss (0.02–0.05) was observed in Al_{0.02}Nb_{0.05}Sn_{0.93}O₂ and Al_{0.03}Nb_{0.05}Sn_{0.92}O₂ ceramics across a wide range of frequencies and temperatures. The large difference in resistance and conductive activation energy between grains and grain boundaries indicates that the internal barrier layer capacitor (IBLC) effect may be responsible for the CP.

The Al + Nb co-doped SnO₂ samples were synthesized using the standard conventional solid-state reaction process, where rutile SnO₂ (99.9%; Alfa Aesar), Nb₂O₅ (99.9%; Alfa Aesar), and Al₂O₃ (99.9%; Alfa Aesar) powders were used as precursors. The powders were mixed and then pressed into a disk. The temperature was increased at a rate of 2 °C/min, and the disk was sintered at 1500 °C in air for 20 h. The X-ray diffraction (XRD) patterns of the Al_xNb_{0.05}Sn_{0.95-x}O₂ ceramics acquired using a PANalytical X'PERT PRO powder diffractometer indicated that all ceramics were in the pure rutile phase, as shown in Fig. S1 (supplementary material). The microstructure was investigated with the scanning electron microscopy (Ultra55, Carl ZeissNTS GmbH). Figs. S2 and S3 (supplementary material) show the scanning electron microscope (SEM) images and the energy dispersive X-ray spectroscopy (EDX) results, respectively, for Al_xNb_{0.05}Sn_{0.95-x}O₂ (x = 0.01, 0.03, 0.05, and 0.07) ceramic surfaces. The smallest grain size (<1 μm) was obtained for the sample with x = 0.01, and the grain size increased with Al doping. The dielectric properties and the impedance spectroscopy were measured

^{a)} Authors to whom correspondence should be addressed. Electronic addresses: wangxianjie@hit.edu.cn; suiyu@hit.edu.cn; and songbo@hit.edu.cn

using Agilent 4980A in the Physical Property Measurement System and a stove at low and high temperature, respectively. The room-temperature (RT) dielectric properties were measured at high frequencies using the Agilent 4292A precision impedance analyzer.

Fig. 1 shows the dielectric permittivity and loss of $\text{Al}_x\text{Nb}_{0.05}\text{Sn}_{0.95-x}\text{O}_2$ ceramics at room temperature. CP (3×10^3) was observed along with high dielectric loss in Nb-doped SnO_2 ceramics. Al doping effectively reduces the dielectric loss, with the lowest dielectric loss value observed for Al doping levels of 2% and 3%. Further increases in the Al doping concentration ($>4\%$) led to an observed increase in the dielectric loss and a plateau in the dielectric permittivity. The frequency at which the dielectric permittivity plateau appears gradually decreased with increasing Al doping concentration. The dielectric permittivity and loss data at 1 kHz, 10 kHz, 100 kHz, and 1 MHz at 300 K and 350 K are shown in Fig. S4 (supplementary material).³⁰ The frequency independence of the CP and low loss were observed in $\text{Al}_x\text{Nb}_{0.05}\text{Sn}_{0.95-x}\text{O}_2$ ($x = 0.01, 0.02, \text{ and } 0.03$) ceramics. In the frequency range from 1 kHz to 1 MHz, the dielectric losses were approximately 0.03 and 0.02 in $\text{Al}_{0.03}\text{Nb}_{0.05}\text{Sn}_{0.92}\text{O}_2$ and $\text{Al}_{0.02}\text{Nb}_{0.05}\text{Sn}_{0.93}\text{O}_2$ ceramics, respectively, which are much lower than that observed in CCTO,¹⁷ co-doped TiO_2 ,^{21,30} and doped NiO.¹² Although lower dielectric loss values have been reported in doped CCTO¹⁷ and $\text{Y}_{2/3}\text{Cu}_3\text{Ti}_4\text{O}_{12}$,¹⁸ these low dielectric loss values are only observed in a narrow frequency range, just like for $\text{Al}_{0.01}\text{Nb}_{0.05}\text{Sn}_{0.96}\text{O}_2$ ceramics.

The temperature dependence of the dielectric permittivity and dielectric loss of $\text{Al}_{0.02}\text{Nb}_{0.05}\text{Ti}_{0.93}\text{O}_2$ at various frequencies is shown in Fig. 2. CP ($>10^3$) was observed in a broad range of temperatures from 100 K to 450 K. The dielectric permittivity increased dramatically, from 10^1 to 10^3 , with increasing temperature to 100 K, after which another dielectric permittivity plateau appeared as the temperature increased to 450 K. The temperature dependence of the dielectric permittivity in the temperature range from 100 K to 450 K is very weak, which is quite similar to the behavior observed in CCTO³¹ and co-doped TiO_2 ceramics.³⁰ Interestingly, a low dielectric loss was observed for temperatures from 140 K to 400 K. The relaxation time τ can be calculated from the imaginary part of the dielectric

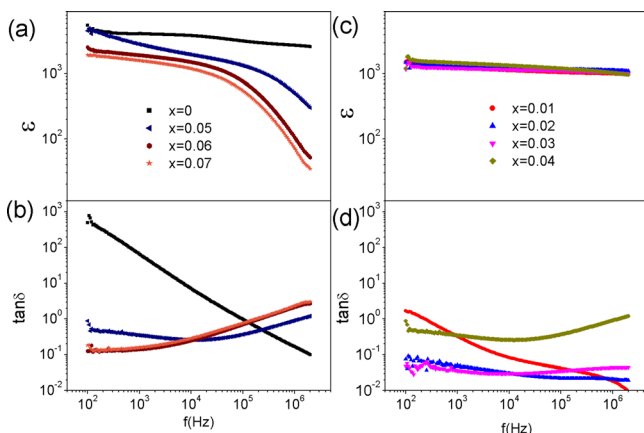


FIG. 1. Dielectric permittivity and loss of $\text{Al}_x\text{Nb}_{0.05}\text{Sn}_{0.95-x}\text{O}_2$ ceramics at room temperature.

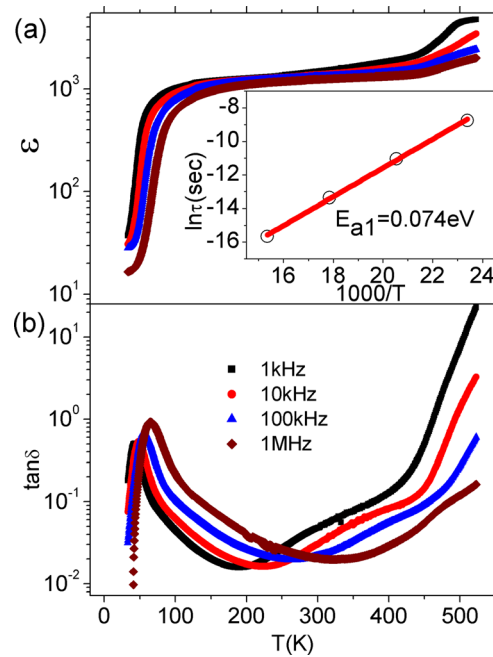


FIG. 2. Dielectric permittivity (a) and loss (b) of $\text{Al}_{0.02}\text{Nb}_{0.05}\text{Sn}_{0.93}\text{O}_2$ ceramics as a function of temperature. The inset of (a) shows the relaxation time at low temperature.

permittivity using $2\pi\tau f_p = 1$, where f_p is the frequency at which the imaginary part of the dielectric permittivity is a maximum. The temperature dependence of τ can be described by the following formula:²

$$\tau = \tau_0 \exp\left(\frac{E_{a1}}{k_B T}\right), \quad (1)$$

where τ_0 is a constant, E_{a1} is the conductive activation energy of the grain, k_B is the Boltzmann constant, and T is the temperature. The temperature dependence of τ is shown in the inset of Fig. 2. The conductive activation energy of the grain in $\text{Al}_{0.02}\text{Nb}_{0.05}\text{Sn}_{0.93}\text{O}_2$ ceramics was calculated to be 0.074 eV using Eq. (1), which is on the same order of magnitude as the grain conductive activation energy in CCTO¹¹ and co-doped TiO_2 ³⁰ ceramics.

The capacitance determined from the fit to the impedance spectra of $\text{Al}_{0.02}\text{Nb}_{0.05}\text{Sn}_{0.93}\text{O}_2$ ceramics at high temperatures was 0.2 nF cm, as shown in Fig. 3. The relative

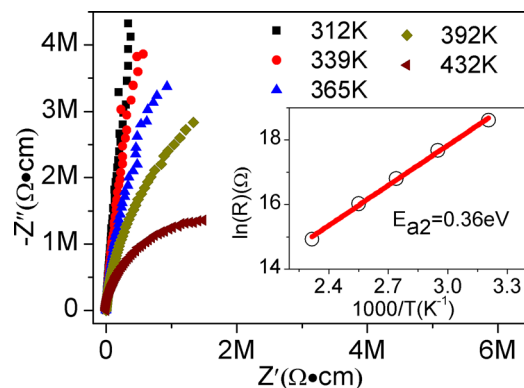


FIG. 3. Complex plane plot of impedance of $\text{Al}_{0.02}\text{Nb}_{0.05}\text{Sn}_{0.93}\text{O}_2$ ceramics at high temperature. The inset shows the temperature dependence of grain boundary resistance.

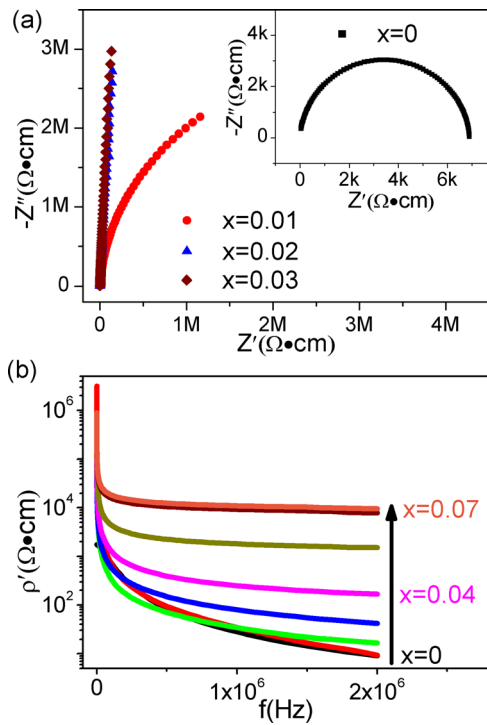


FIG. 4. (a) Complex plane plot of impedance of $\text{Al}_x\text{Nb}_{0.05}\text{Sn}_{0.95-x}\text{O}_2$ ceramics at room temperature. (b) The real part of the resistivity of $\text{Al}_x\text{Nb}_{0.05}\text{Sn}_{0.95-x}\text{O}_2$ ceramics as a function of frequency.

intrinsic dielectric permittivity of CCTO is 80, and the typical capacitance of the grain boundary is 1–10 nF cm.¹¹ The relative dielectric permittivity of pure rutile SnO_2 is only 12, which is much smaller than that of CCTO. These results suggest that the arc shown in Fig. 3 can be attributed to the grain boundary response of Al + Nb co-doped SnO_2 . The grain boundary resistance decreased with increasing temperature, and their relationship can be described by the following formula:¹¹

$$R = R_0 \exp\left(\frac{E_{a2}}{k_B T}\right), \quad (2)$$

where R is the resistance, R_0 is a constant, and E_{a2} is the conductive activation energy of the grain boundary. The conductive activation energy of the grain boundary was calculated to be 0.36 eV, which is consistent with those of co-doped TiO_2 (Ref. 30) and CCTO¹¹ CP ceramics. In the oxide semiconductors, oxygen vacancies are easily introduced into the grain instead of the grain boundary in sintering processes at high temperature. The resistivity can be effectively improved by suppressing the production of oxygen vacancies because a small amount of oxygen loss generated during high-temperature sintering, in the order of 100 ppm, could lead to an n-type semiconductivity.³² Therefore, the E_a of the grain can be attributed to the interaction between doped Nb and

oxygen vacancies, and the E_a of the grain boundary is a typical band gap for a doped semiconductor,^{21,33} which can be attributed to the impurity energy level introduced by doped Nb, which is considered donor doping. The huge difference in conductive activation energy between grains and grain boundaries indicates that the internal barrier layer capacitor (IBLC) effect may be responsible for the CP in Al + Nb co-doped SnO_2 ceramics. In addition, the second dielectric plateau in Fig. 2 at the high-temperature range can be attributed to the surface barrier layer capacitor (SBLC) effect, as observed in In + Nb co-doped TiO_2 samples.³⁰

We investigated the influence of Al-Nb co-doping on the resistance of the grains and grain boundaries to explain the dielectric properties, as the resistance of the grains and grain boundaries plays an important role in the dielectric behaviors in CP ceramics with an IBLC effect.^{21,29} The valence state configurations of Al, Sn, and Nb in Al + Nb co-doped SnO_2 are +3, +4, and +5, respectively. Therefore, Nb doping in SnO_2 can be considered donor doping and introduces many n-type carriers. Meanwhile, Al doping in SnO_2 can be considered acceptor doping and can capture the electrons introduced by Nb doping, increasing the resistance of the grain and grain boundary. Therefore, the concentration of carriers and the resistance of the grains and grain boundaries can be acutely tuned by varying the ratio between Nb and Al cations, which will result in CP and low dielectric loss in co-doped SnO_2 .

The complex plane plots of the room temperature (RT) impedance of $\text{Al}_x\text{Nb}_{0.05}\text{Sn}_{0.95-x}\text{O}_2$ ceramics ($x = 0.01, 0.02$, and 0.03) are shown in Fig. 4(a), with the data for $x = 0$ shown in the inset. The grain boundary response arc can be identified clearly, and the calculated resistivity of the grain boundary is shown in Table I. The grain boundary resistivity was too large to be fit using a complex impedance at RT for the samples with $x \geq 0.04$, so the complex impedance at higher temperatures, as shown in Fig. S5 (supplementary material), was used to calculate the resistivity of the grain boundary at RT according to Eq. (2) for $x = 0.04$ ceramics.³⁰ The increase in grain boundary resistivity with increasing Al doping confirms that the lower dielectric loss in Al + Nb co-doped SnO_2 can be attributed to the increasing grain boundary resistance with Al doping.²¹ The frequency dependence of the real part of the RT resistivity for $\text{Al}_x\text{Nb}_{0.05}\text{Sn}_{0.95-x}\text{O}_2$ ceramics is shown in Fig. 4(b). The conductivity at high frequency is dominated by the grain conductance.²¹ With increasing Al doping, grain resistance increases, as shown in Fig. 4(b) and Table I. The large difference between grain resistance and grain boundary resistance indicates that the IBLC effect is responsible for the CP in Al + Nb co-doped SnO_2 ceramics.

The dielectric loss is also strongly affected by the relaxation time. The relaxation time τ was determined from the

TABLE I. Grain and grain boundary resistivity of $\text{Al}_x\text{Nb}_{0.05}\text{Sn}_{0.95-x}\text{O}_2$ at room temperature.

x	0	0.01	0.02	0.03	0.04	0.05	0.06	0.07
R_{gb} (Ω cm)	6911	5.73×10^6	9.59×10^7	3.06×10^8	5.60×10^{10}
R_g (Ω cm)	9.09	9.34	16.69	41.76	165.91	1502.11	7869.91	9543.97

grain resistance R_g and grain boundary capacitance C_{gb} and can be described by the following formula:

$$\tau = C_{gb}R_g. \quad (3)$$

Furthermore, the relationship between the relaxation time τ and frequency at which the peak dielectric loss occurs (f_p) is $2\pi\tau f_p = 1$. τ increases with increasing R_g , which suggests that f_p gradually shifts to lower frequencies with increasing R_g . A step in the dielectric permittivity is clearly observed when the Al doping content is greater than 0.05, and the frequency where the dielectric permittivity begins to drop decreases with increasing R_g (as shown in Fig. 1). Therefore, the increasing grain resistance may be responsible for the higher dielectric loss as well as the strong frequency dependence of the dielectric permittivity and loss. To verify this conjecture, the dielectric permittivity and loss were measured at frequencies up to 100 MHz at RT. As shown in Fig. 5, the dielectric permittivity plateau and dielectric loss peak can be observed in the $\text{Al}_x\text{Nb}_{0.05}\text{Sn}_{0.95-x}\text{O}_2$ ceramics ($x = 0.04, 0.05, \text{ and } 0.06$). A dramatic drop in the dielectric permittivity (from 10^3 to 10^1) and higher dielectric loss were observed across a wide range of frequencies around the loss peak. More importantly, the dielectric loss peak shifted to lower frequencies with increasing Al doping content, which indicates that the relaxation time τ increases with increasing grain resistance. The high-frequency experimental data corroborates our conjecture that the increase in the dielectric loss for Al doping content over 3% can be attributed to the larger grain resistance at higher Al-doping levels.

In summary, we have reported CP and low loss in Al + Nb co-doped rutile SnO_2 ceramics across a broad range of frequencies and temperatures. Al + Nb co-doped SnO_2 ceramics exhibit lower dielectric loss than traditional non-ferroelectric CP materials, with an excellent independence of frequency/temperature. The large differences in the

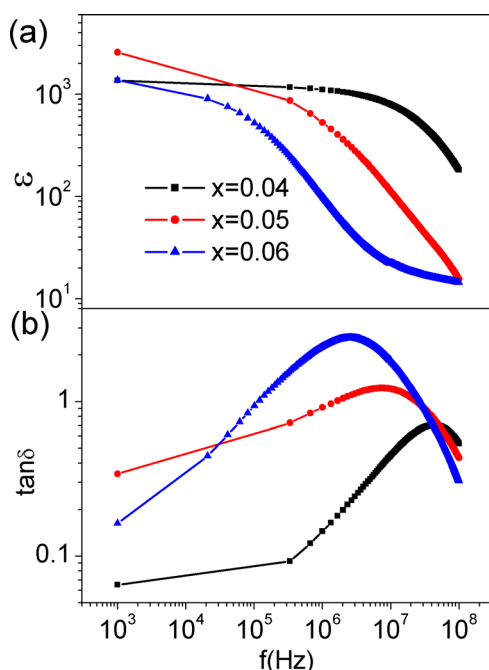


FIG. 5. Dielectric permittivity (a) and loss (b) of $\text{Al}_x\text{Nb}_{0.05}\text{Sn}_{0.95-x}\text{O}_2$ ($x = 0.04, 0.05, \text{ and } 0.06$) ceramics at frequencies up to 100 MHz.

resistance and conductive activation energy between the grain and grain boundary suggest that the IBLC effect is responsible for the CP. Al doping can modulate the dielectric behavior by increasing grain and grain boundary resistances. The increase in grain boundary resistance can effectively reduce dielectric loss; meanwhile, the increasing grain resistance will increase the relaxation time τ , resulting in a higher dielectric loss when the Al doping level exceeds 0.04.

See [supplementary material](#) for figures.

This work is supported by the National Natural Science Foundation of China (Nos. 51472064, 51372056, 11304060, 61308052, 51672057), the Science and Technology Innovation Talent Foundation of Harbin (2012RFXXG110), the Fundamental Research Funds for the Central Universities (Grant Nos. HIT.BRETI.201220, HIT.NSRIF.2012045, HIT.ICRST.2010008), the Program for Innovation Research of Science in Harbin Institute of Technology (PIRS of HIT 201616), the International Science & Technology Cooperation Program of China (2012DFR50020) and the Program for New Century Excellent Talents in University (NCET-13-0174).

¹S. Krohns, P. Lunkenheimer, S. Meissner, A. Reller, B. Gleich, A. Rathgeber, T. Gaugler, H. U. Buhl, D. C. Sinclair, and A. Loidl, *Nat. Mater.* **10**, 899 (2011).

²C. C. Homes, T. Vogt, S. M. Shapiro, S. Wakimoto, and A. P. Ramirez, *Science* **293**, 673 (2001).

³C. C. Homes and T. Vogt, *Nat Mater.* **12**, 782 (2013).

⁴Z. H. Gai, Z. X. Cheng, X. L. Wang, L. L. Zhao, N. Yin, R. Abah, M. L. Zhao, F. Hong, Z. Y. Yu, and S. X. Dou, *J. Mater. Chem. C* **2**, 6790 (2014).

⁵A. R. West, T. B. Adams, F. D. Morrison, and D. C. Sinclair, *J. Eur. Ceram. Soc.* **24**, 1439 (2004).

⁶M. T. Buscaglia, M. Viviani, V. Buscaglia, L. Mitoseriu, A. Testino, P. Nanni, Z. Zhao, M. Nygren, C. Harnagea, D. Piazza, and C. Galassi, *Phys. Rev. B* **73**, 064114 (2006).

⁷B. N. Rao, R. Datta, S. S. Chandrashekar, D. K. Mishra, V. Sathe, A. Senyshyn, and R. Ranjan, *Phys. Rev. B* **88**, 224103 (2013).

⁸M. Matsubara, T. Yamaguchi, W. Sakamoto, K. Kikuta, T. Yogo, and S. Hirano, *J. Am. Ceram. Soc.* **88**, 1190 (2005).

⁹S. X. Zhao, Q. Li, Y. C. Feng, and C. W. Nan, *J. Phys. Chem. Solids* **70**, 639 (2009).

¹⁰S. J. Zhang and F. Li, *J. Appl. Phys.* **111**, 031301 (2012).

¹¹D. C. Sinclair, T. B. Adams, F. D. Morrison, and A. R. West, *Appl. Phys. Lett.* **80**, 2153 (2002).

¹²J. Wu, C. W. Nan, Y. Lin, and Y. Deng, *Phys. Rev. Lett.* **89**, 217601 (2002).

¹³S. Krohns, P. Lunkenheimer, C. Kant, A. V. Pronin, H. B. Brom, A. A. Nugroho, M. Diantoro, and A. Loidl, *Appl. Phys. Lett.* **94**, 122903 (2009).

¹⁴J. Rivas, B. Rivas-Murias, A. Fondado, J. Mira, and M. A. Se naris-Rodr guez, *Appl. Phys. Lett.* **85**, 6224 (2004).

¹⁵M. E. Abrishami, A. Kompany, and S. M. Hosseini, *J. Electroceram.* **29**, 125 (2012).

¹⁶X. H. Li, L. Xu, L. X. Liu, Y. Wang, X. X. Cao, Y. J. Huang, C. M. Meng, and Z. G. Wang, *J. Mater. Chem. A* **2**, 16740 (2014).

¹⁷L. Ni and X. M. Chen, *Solid State Commun.* **149**, 379 (2009).

¹⁸P. F. Liang, Z. P. Yang, and X. L. Chao, *J. Alloys Compd.* **678**, 273 (2016).

¹⁹W. Hu, Y. Liu, R. L. Withers, T. J. Frankcombe, L. Noren, A. Snashall, M. Kitchin, P. Smith, B. Gong, H. Chen, J. Schiemer, F. Brink, and J. Wong-Leung, *Nat. Mater.* **12**, 821 (2013).

²⁰J. L. Li, F. Li, C. Li, G. Yang, Z. Xu, and S. J. Zhang, *Sci. Rep.* **5**, 8295 (2015).

²¹J. L. Li, F. Li, Y. Y. Zhuang, L. Jin, L. H. Wang, X. Y. Wei, Z. Xu, and S. J. Zhang, *J. Appl. Phys.* **116**, 074105 (2014).

²²Y. Q. Wu, X. Zhao, J. L. Zhang, W. B. Su, and J. Liu, *Appl. Phys. Lett.* **107**, 242904 (2015).

- ²³X. H. Wei, W. J. Jie, Z. B. Yang, F. G. Zheng, H. Z. Zeng, Y. Liu, and J. H. Hao, *J. Mater. Chem. C* **3**, 11005 (2015).
- ²⁴J. A. Aguilar-Martínez, M. B. Hernández, A. B. Glot, and M. I. Pech-Canul, *J. Phys. D: Appl. Phys.* **40**, 7097 (2007).
- ²⁵L. Bai, Y. G. Wu, and L. Zhang, *J. Alloys Compd.* **661**, 6 (2016).
- ²⁶J. L. Li, F. Li, Z. Xu, Y. Y. Zhuang, and S. J. Zhang, *Ceram. Int.* **41**, S798 (2015).
- ²⁷P. Qi, J. F. Wang, W. B. Su, H. C. Chen, G. Z. Zhang, C. M. Wang, and B. Q. Ming, *Mater. Sci. Eng. B* **119**, 94 (2005).
- ²⁸K. Rajwali and M. H. Fang, *Chin. Phys. B* **24**, 127803 (2015).
- ²⁹Y. L. Song, X. J. Wang, X. Q. Zhang, Y. Sui, Y. Zhang, Z. G. Liu, Z. Lv, Y. Wang, P. Xu, and B. Song, *J. Mater. Chem. C* **4**, 6798 (2016).
- ³⁰Y. L. Song, X. J. Wang, Y. Sui, Z. Y. Liu, Y. Zhang, H. S. Zhan, B. Q. Song, Z. G. Liu, Z. Lv, L. Tao, and J. K. Tang, *Sci. Rep.* **6**, 21478 (2016).
- ³¹M. Li, Z. J. Shen, M. Nygren, A. Feteira, D. C. Sinclair, and A. R. West, *J. Appl. Phys.* **106**, 104106 (2009).
- ³²F. D. Morrison, D. C. Sinclair, and A. R. West, *J. Am. Ceram. Soc.* **84**, 474 (2001).
- ³³D. W. Johnson, L. E. Cross, and F. A. Hummel, *J. Appl. Phys.* **41**, 2828 (1970).